MAL: High performance method for loading hydrophobic molecular materials into MCM-41 mesoporous silica – Analysis of confined L-tryptophan by Raman spectroscopy

Basma Moutamenni, Nicolas Tabary, Laurent Paccou, Yannick Guinet, Alain Hedoux

MAL: high performance method for loading hydrophobic molecular materials into MCM-41 mesoporous silica – Analysis of confined L-tryptophan by Raman spectroscopy

Basma Moutamenni, Nicolas Tabary, Laurent Paccou, Yannick Guinet, Alain Hédoux*

Univ. Lille, CNRS, INRAE, Centrale Lille, UMR 8207 - UMET - Unité Matériaux et Transformations, F-59000 Lille, France

Abstract

The capabilities of the recent MAL (Milling-Assisted Loading) method were analyzed for the geometric confinement of amino acids within mesoporous silica matrices. The present study has shown a high filling degree (45 wt%) of L-tryptophan into unmodified MCM-41 pores. It was shown that the low-frequency Raman spectroscopy is a suited technique to determine that molecular materials are actually confined into silica-based ordered mesoporous materials from the analysis of lattice mode region, and to probe the molecular conformation of confined materials and their interaction with the pore surface from the analysis of internal vibrations.

Keywords: Nanoconfinement – amino acids – ordered mesoporous silica – Low-frequency Raman spectroscopy – loading methods

* Corresponding author: alain.hedoux@univ-lille.fr

1. Introduction

Ordered mesoporous silicas (MPS) have considerably focused analyzes over the past twenty [1, 2] years, especially in the pharmaceutical area serving as drug-delivery systems (DDS). These DDS provide two considerable advantages. The first is inherent to the physical state (amorphous or nanocrystals) of pharmaceutical ingredients (APIs) confined at the nanoscale, providing enhanced bioavailability and physical stability[3]. The second advantage is related to their inorganic nature permitting them to overcome physiologic barriers, for delivering the active APIs on the targeted site. On the other hand, their weak loading capacity was considered as an insurmountable obstacle to their development [3, 4]. Moreover, the common loading methods require the use of toxic solvents. Consequently, a considerable attention has been paid to the loading methods [5, 6] in order to overcome these inconveniences unacceptable for the therapeutic use. Loading methods can be classified in two categories: solvent-free methods and solvent-based methods [6]. Despite they required organic solvents, often inconsistent with therapeutic applications, the most commonly used are solvent-based methods i.e. adsorption [7], incipient wetness impregnation [8], solvent evaporation [9]. More recently, co-spray drying [10], diffusion supported loading methods have been developed [11]. Solvent-free methods are less widely used, despite a better compatibility with the therapeutic application. Melt method [12] can be considered as very efficient but only for low-T_m APIs [13], melting of high-T_m APIs could be responsible for chemical degradation. It was shown that physical mixing gives the opportunity to load easily APIs within mesoporous silica matrices [14]. Interestingly, the authors have recently introduced an innovative method for loading APIs within mesoporous silicas at the solid state [15]. This MAL (milling-assisted loading) method gives the opportunity to overcome the obstacles to the therapeutic use of MPS as DDS. It was shown[15] that co-milling MPS with APIs for 30 minutes maximum makes possible the loading of a large amount of APIs (35 to 40 wt%) while preserving the ordered structure of MPS, without use of organic solvents. Consequently, this green loading method provides opportunities for developing MPS as DDS. Additionally, selecting the pore geometry (pore diameter) makes possible to manipulate the physical state of ibuprofen[16]. A subtle tuning of the average pore diameter from 6 to 9 nm induces the presence of nanocrystals coexisting with amorphous ibuprofen, with a significant impact on the drug release profiles [16]. Besides the great impact of MAL method on the DDS development, it was shown that this loading method makes possible to explore new routes (phase transformations) to achieve new physical states, only existing under confinement at the nanoscale [17, 18]. The fundamental difference between MAL and impregnation methods is related to the physical state of the confined materials. Co-milling of MPS and molecular materials induces the confinement of pre-existing nuclei which can growth. That makes possible crystallization under severe spatial restriction bypassing the nucleation stage, not possible with impregnation methods. The growth and stability of nanocrystals are then controlled by the pore geometry.

The next step in the development of the MAL method consists to optimize the confinement of peptides and proteins by MAL for delivering biopharmaceuticals considered as the medicines of the future. One of the most advanced biomedical applications concerns the

delivery of proteins for bone tissue regeneration [19, 20]. In this context, the confinement of L-tryptophan (L-Trp) by MAL was analyzed as model systems present in the three-dimensional structure of a large variety of proteins. However, the hydrophobicity of L-Trp requires the chemical modification of the pore wall for achieving a significant loading capacity [19, 20]. In this study, we used unmodified MCM-41 matrices to estimate the loading capacity of hydrophobic materials by MAL.

Among the large variety of experimental techniques used for probing confined materials, most of which being probes of the physical state, except thermogravimetry analysis (TGA) [16] and gas sorption. It is worth noting that gas sorption provides important data on surface area and porosity (distribution of pore size) of mesoporous silica [21]. Microscopy [22] (SEM, TEM, AFM) are also used for providing information relative to morphology and geometry of pores. Obtaining information on the physical state of APIs is more difficult given the sample preparation required for the analysis and the destructive nature of the electron radiation for organic compounds, especially in the case of TEM. Differential scanning calorimetry (DSC) [16, 23], X-ray diffraction [16, 23], NMR spectroscopy [24-27] and vibrational spectroscopy (Infrared [28] and Raman [15, 29]) are the most used techniques for analyzing the physical state of APIs, also providing additional information on the filling degree of pores and the physical stability of confined APIs. In order to obtain the broadest spectrum of information on confined materials including the filling degree, the physical state of the confined material and the interactions between confined material and pore surface, Raman spectroscopy was selected. First, Raman spectroscopy doesn't request any specific sample preparation making possible spectrum acquisition five minutes maximum after obtaining composites by MAL method. Additionally, spectra were collected in a wide frequency range provide information in both the lattice mode region and the molecular fingerprint region. The low-frequency region was previously used for determining the loading capacity of SBA-15 with ibuprofen and indomethacin using MAL [15] by discriminating amorphous state from crystallites, the presence of amorphous matter being indicative of confinement. It was previously shown that low-frequency Raman spectroscopy is a very sensitive tool for detecting and identifying subtle crystalline signatures developing from the early stages of crystallization, spatially restricted within a few tens of nanometers [30-32]. At higher frequencies, the molecular fingerprint region (600 – 1800 cm^{-1}) provides information on the possible conformational modifications of confined molecules and also on the interaction strength between pore walls and confined materials. The very weak Raman signal of MPS [15, 17, 18] is also a major advantage for analyzing the physical state of the confined matter and its transformations.

2. Material and Methods

2.1.Sample preparation

L-Tryptohan ($C_{11}H_{12}N_2O_2$, L-Trp) was purchased from Sigma-Aldrich (purity higher than 98%) was used as received.

Aerosil was purchased from Sigma-Aldrich (SiO_2, S_{BET} = 175-225 m^2/g) and used as is. MCM-41, CAS number: 112-02-7, (S_{BET} = 1033 m^2/g, total pore volume V_{abs} = 1.18 cm^3/g, and pore size D_p = 3.6 nm) was purchased from Sigma-Aldrich. Additional information can be found in a recent paper [17].

MAL method consists in co-milling L-Trp and MCM-41 solid mixtures, systematically performed at 30 Hz at room temperature for 30 minutes, using a Mixer Mill (MM400/Retsch). In this method, L-Trp is placed with MCM-41 and one steel ball (Ø=7mm) inside an Eppendorf tube (5ml) vibrating at 30 Hz. To avoid any overheating of L-Trp, milling periods (5 min) were alternated with pause periods (2 min). The total amount of (**x**wt L-Trp : (1-**x**) wt MCM-41) samples, with $0.30 \leq x \leq 0.5$, was estimated in order to fill in more than a third of the volume of the Eppendorf tube corresponding to a constant total mass of 200 mg. Composites were directly analyzed by low and high-frequency Raman spectroscopy after stopping the milling and removing powder samples out of the jar, without any additional sample preparation.

Cryomilling of L-Trp in the bulk form was performed with a cryogenic mill (Retsch cryomill), composed of an Agate jar (80ml) and a ball (Ø=21mm). The vial containing 1g of the sample is immersed in liquid nitrogen. Shuttling frequency corresponding to presented results was of 30 Hz. To avoid mechanical heating, a pause of 2min was applied between each period of 5 min of cryomilling) The total duration of imposed cryomilling was 30 min.

2.2.Raman spectroscopy

Low-wavenumber Raman spectra were collected using a high-resolution Raman XY-Dilor spectrometer to analyze the non-polarized back-scattered light. The spectrometer is composed of three gratings characterized by a focal length of 800 mm. The choice of experimental conditions (incident radiation, entrance and exit slit width opened at 200 μm) gives a spectral resolution of about 1 cm^{-1} in the 5 – 250 cm^{-1} region, and allows the rejection of exciting light (the 660 nm line of a solid diode laser) down to 5 cm^{-1}. The spectrometer is equipped with a liquid nitrogen cooled charge coupled device detector. The high sensitivity of the detector and the large analyzed scattered volume (~ 0.5 cm^3) allow us to record low-wavenumber Raman spectra in the 5 – 250 cm^{-1} range in 5 minutes.

Raman spectra in the molecular fingerprint region were collected using a Renishaw In Via micro-Raman spectrometer equipped with a 785 nm laser diode. An achromatic lens was used to focus the laser beam on the composite and to collect the 180° scattered light in order to analyze the largest possible volume of the sample.

3. Results and discussion

3.1.Low-frequency Raman investigations.

It was previously shown that a signature of confinement of molecular materials at the nanoscale by MAL was the detection of amorphous matter [15-17]. Consequently, the spectra of crystalline and amorphous L-Trp were collected in the low-frequency to be used as references for determining the nature of the physical state of L-Trp after co-milling with MCM-41. It is recognized [33] that milling molecular materials at temperatures well below T_g is a rapid and safe route for achieving the amorphous state, avoiding chemical degradation of high-T_m materials. L-Trp was then milled at low-temperature (liquid nitrogen temperature) for 30 minutes. The spectrum was recorded at room temperature with an acquisition time of 5 min. The spectrum was plotted in Figure 1a after conversion of Raman intensity into reduced intensity according to:

$$I_r(\omega) = \frac{I_{Raman}(\omega,T)}{[n(\omega+1)]\omega} \qquad (1)$$

where n(ω) is the Bose-Einstein occupation factor. This transformation is required to avoid the band-shape distortion in the low-frequency region induced by temperature fluctuations. The spectrum plotted in Figure 1a is typical of an amorphous state, characterized by the absence of phonon peaks corresponding lattice vibrations, and the presence of a Rayleigh wing distinctive of quasielastic scattering (QES). Very disordered states in molecular materials are characterized by the overlapping of the QES contribution with vibrational components. To obtain a structural information representative of the short-range order in amorphous states, the QES contribution must be removed from the reduced intensity, and

$I_r(\omega)$ can be then converted into Raman susceptibility ($\chi"(\omega)$) directly related to the vibrational density of states (VDOS, $G(\omega)$), according to [34, 35]:

$$\chi"(\omega) = \omega . I_r(\omega) = \frac{C(\omega)}{\omega} . G(\omega) \qquad (2)$$

where $C(\omega)$ is the light-vibration coupling coefficient, which can be determined from inelastic neutron scattering experiments [36, 37], and often exhibits a linear ω-dependence in the very low-frequency region in various molecular materials [36, 38]. The Raman susceptibility is then recognized as a very close representation of the VDOS with a spectral resolution significantly higher than that of $G(\omega)$ determined from inelastic neutron scattering data [36]. Determining the QES contribution requires the fitting procedure described in Figure 1a. The QES is usually described by a Lorentzian shape centered at zero. The vibrational component located at the lowest frequencies is assigned to the Boson peak (BP), recognized as the universal vibrational signature of the amorphous state [36, 39] and associated to the deviation of $G(\omega)$ from the ω^2-behavior, *i.e.* the excess of VDOS in the very low-frequency range. Other additional vibrational components were described by mixed Gaussian-Lorentzian band-shapes. After subtraction of QES from the reduced intensity, $I_r(\omega)$ was converted into $\chi"(\omega)$ according to equation (2). The $\chi"(\omega)$ spectrum was plotted in Figure 1b, and compared with the spectrum of lattice vibrations of crystalline L-Trp. The phonon peaks are the signature of the crystalline symmetry and are only detected for a molecular long-range order with periodic conditions. The band width of phonon peaks is mostly depending on the extension of the long-range order for quasi-harmonic collective motions. In this context, the low-frequency spectra of nanocrystalline states are then resembling spectra of amorphous states [40]. Using Raman spectroscopy in the low-frequency region revealed a distribution of physical states of ibuprofen embedded in SBA-15, from the microcrystalline to the amorphous state via nanocrystals [16].

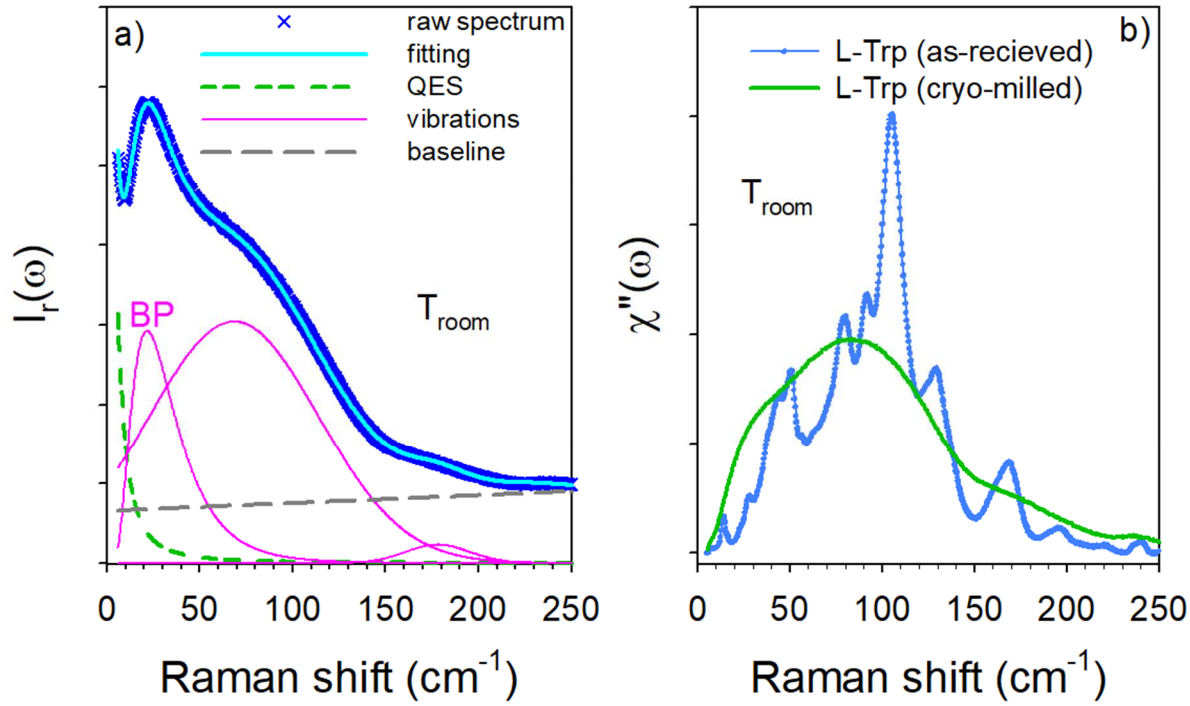

Figure 1 : Low-frequency spectrum of cryomilled L-Trp at room temperature ; a) fitting procedure of the reduced intensity; b) Raman susceptibility spectrum of cryomilled L-Trp compared with the of lattice vibrations in crystalline L-Trp

In a first step the influence of milling for 30 min at 30 Hz on L-Trp at room temperature was analyzed, when L-Trp was milled alone, and milled with aerosil (50 – 50 wt%), the basic component of MCM-41. The low-frequency spectra were plotted in the Raman susceptibility representation in Figure 2 with the spectrum of as-received L-Trp. This comparison indicates a very weak impact of the milling on the physical state of L-Trp when milled alone, and slightly enhanced when it was milled with aerosil. The weak broadening of phonon peaks corresponding to the lattice modes observed after milling reflects a weak reduction of the grain size, as generally observed for Bragg peaks by powder X-ray diffraction, and a marginal influence of aerosil on the physical state of L-Trp during milling for 30 minutes.

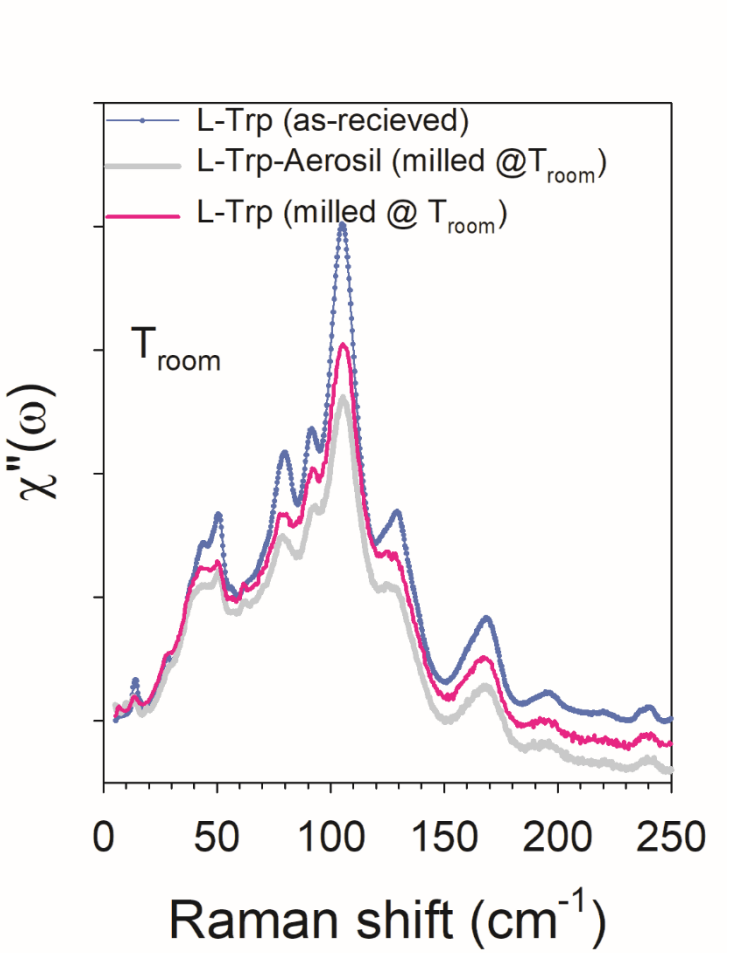

Figure 2 : Raman susceptibility spectra of L-Trp milled at room temperature alone and comilled with aerosil, compared with the spectrum of L-Trp (as-received); spectra were arbitrarily shifted along the Y axis for better clarity

In a second step, freshly prepared (L-Trp:MCM-41) composites were analyzed for various L-Trp concentrations ranging from 30 wt% up to 50 wt%. Spectra of freshly prepared composites were plotted in Figure 3 in Raman susceptibility representation by step of 5 wt% L-Trp. It is clearly observed that all Raman spectra plotted in Figure 3a are similar to the spectrum of cryo-milled L-Trp, with subtle structuration located within the frame in Figure 3, reminiscent of the crystal and indicating a nano-structured state very close to the amorphous state. Given that milling L-Trp (without or with aerosil) does not induce so important spectral changes, these spectra indicate that the physical state of L-Trp within the composites is nanocrystallized. A detailed inspection of spectra plotted in Figure 3b without shift along the Y-axis, clearly shows that the crystalline signature of L-Trp increases from 45% of L-Trp indicating the filling limit of loading L-Trp inside MCM-41 pores close to 45 %.

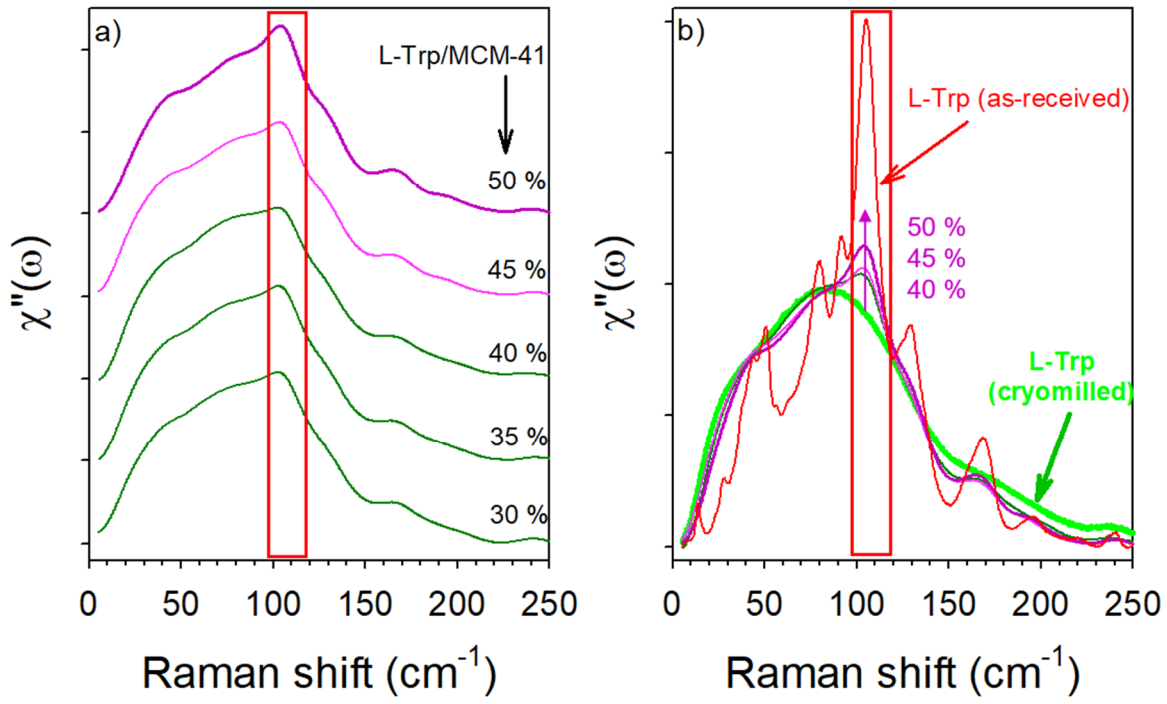

Figure 3 : Raman spectra of L-Trp:MCM-41 composites at various mass concentrations of L-Trp ranging from 30 to 50 %. The red box highlights the most intense signature of crystalline L-Trp; a) Spectra are arbitrarily shifted along the y-axis for better clarity; b) Spectra of composites ranging from 40 to 50 % of L-Trp are compared with spectra of amorphous and crystalline L-Trp, to show the increase of the crystalline signature from 45 % of L-Trp.

3.2.High-frequency Raman investigations.

The molecular fingerprint region was used to analyze the molecular conformation of L-Trp under confinement, and to probe the interaction between L-Trp and the pore surface. As for low-frequency investigations, the spectra of as-received L-Trp, cryo-milled L-Trp and L-Trp milled at room temperature, were compared in the 800 – 1650 cm^{-1} region in Figure 4. The spectrum of amorphous L-Trp appears as the broadened spectrum of the crystal, as it can be expected for a very disordered state. This broadening is resulting from molecular configurations, inducing breaking of molecular interactions, e.g. H-bonds, responsible for frequency shifts of Raman bands. The 1500 – 1600 cm^{-1} region enlarged in Figure 4b clearly shows both broadening and frequency shifts of Raman bands. DFT calculations using TmoleX software provide the attribution of Raman bands located at 1550 and 1630 cm^{-1}, as corresponding to CH_2 bending and C = O stretching respectively. Note that these vibrations can be affected or coupled with the motions of neighbor atom groups, as observed in amide I bands of proteins [41] mainly corresponding to C=O stretching vibrations with minor contributions of C-N stretching vibration and C-N-H bending motions. This can partly explain the frequency shift between calculated and experimental Raman bands. It is worth noting that both bands can be used to probe molecular associations via H-bonds, NH_2 and C=O groups being involved in H-bonding in the crystal [42]. In this context, the shift toward the high frequencies of the 1630 cm^{-1} band is likely reflecting the break of H-bonds in the amorphous

state, making harder stretching vibrations oppositely to NH_2 bending vibrations the 1550 cm^{-1} shifting toward the low frequencies.

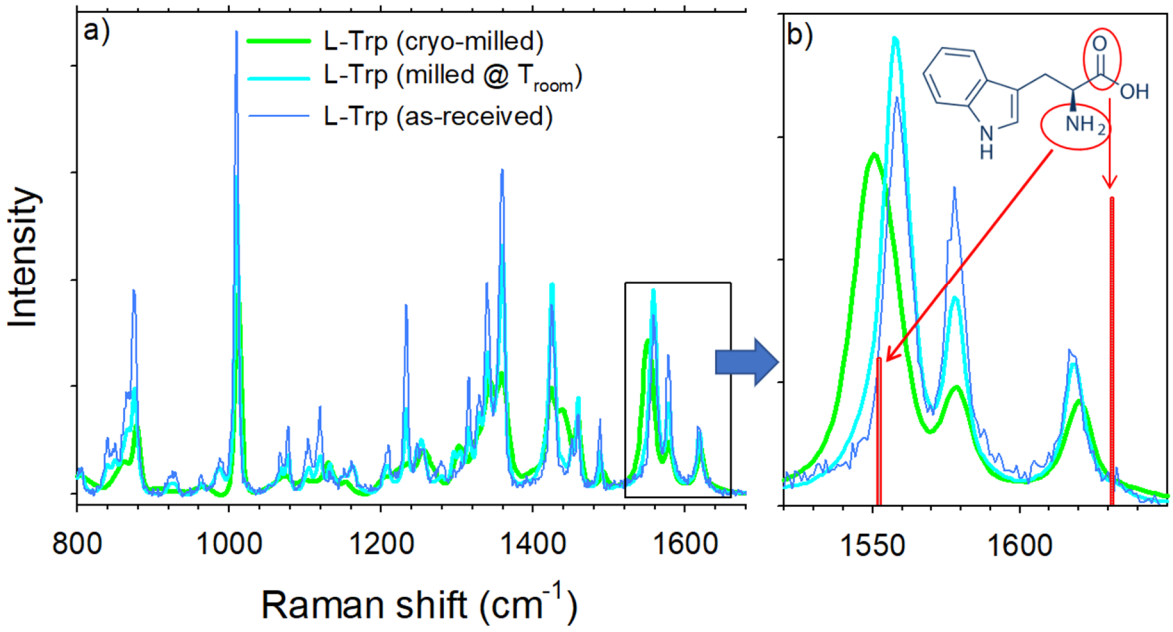

Figure 4 : Raman spectra of as-received L-Trp, cryo-milled L-Trp and L-Trp milled at room temperature a) in the molecular fingerprint region; b) in the 1520 – 1650 cm^{-1} spectral range; vertical bars correspond to calculated frequencies of motions which involve atom groups inside ellipses

The spectrum of amorphous L-Trp was then compared in Figure 5 with the spectrum of the composite containing 40 % of L-Trp. No strong difference can be detected between the spectrum of the amorphous state in the bulk form and the spectrum of the composite, reflecting no change in the molecular conformation of L-Trp under geometric confinement. It is worth noting that this spectral region does not allow to distinguish the amorphous state from the nano-crystallized state. This is an additional validation of the very high sensitivity of the low-frequency region to detect subtle traces of crystallization. However, a detailed inspection of Figure 5b makes possible to detect a shift of the 1630 cm^{-1} band in amorphous L-Trp toward the high frequencies compared to spectrum of the composite. This shift of the C=O stretching band could be considered as the signature of H-bond interactions (C=O…H-O-Si) between L-Trp and the pore surface. It is worth noting that this interaction is relatively weak (weak frequency shift of the 1630 cm^{-1} in composites compared to the bulk form of amorphous L-Trp).

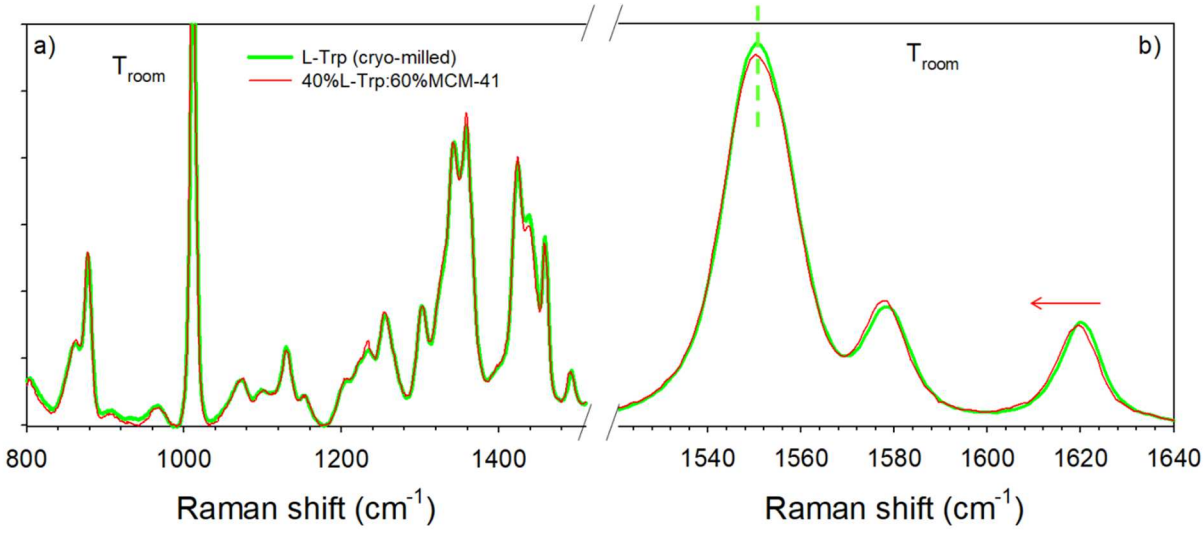

Figure 5 : Comparison between Raman spectra of composite and the bulk form of amorphous L-Trp; a) in the 800 – 1520 cm^{-1} region; b) in the 1520 – 1640 cm^{-1} region; the horizontal arrow shows the frequency shift of the C=O stretching band in the spectrum of the composite considered as a signature of weak interactions between L-Trp and the pore surface.

4. Conclusion

The present study reveals the high performance of MAL method for loading hydrophobic molecular materials into unmodified MCM-41 matrices. About 45 wt% of L-Trp was loaded inside MCM-41 pores, while previously less than 10 wt% can be loaded into modified SBA-15 [10]. It was also shown that only 40 wt% of active pharmaceutical ingredients can be loaded in SBA-15[15, 16] or MCM-41[17]. As it can be expected from its hydrophobic character, L-Trp has weak interactions with the pore surface that can be considered as promoting the filling degree of this amino acid. Given that hydrophobicity is a common property of many essential amino acids, the high filling degree within MPS by MAL could be a general result for amino acids. It can be also expected that this solid-state loading method could be used to confine proteins into MPS matrices. The next stages to this study will be the analysis of the physical stability of amino acids into the pores and the analysis of release profiles.

References.

[1] M. Vallet-Regi, A. Ramila, R.P. Del Real, J. Perez-Pariente, A new property of MCM-41: Drug delivery system, Chem. Mater. 13 (2001) 308-311.
[2] E. Juere, F. Kleitz, On the nanopore confinement of therapeutic drugs into mesopourous silica materials and its implications, Microporous Mesoporous Mater. 270 (2018) 109-119.
[3] S.J. Dengale, H. Grohganz, T. Rades, K. Lobmann, Recent advances in coamorphous drug formulations, Adv. Drug Deliv. Rev. 100 (2016) 116-125.
[4] C.A. Prestidge, T.J. Barnes, C.-H. Lau, C. Barnett, A. Loni, L. Canham, Mesoporous silicon: a platform for the delivery of therapeutics, Expert Opin. Drug Deliv. 4 (2007) 101-110.
[5] K. Trzeciak, A. Chotera-Ouda, I. Bak-Sypien, M. Potrzebowski, Mesoporous silicaparticles as drug delivery systems - The state of the art in loading methods and the recent progress in analytical techniques for monitoring these processes, Pharmaceutics 13 (2021) 950.
[6] K.B. Seljak, P. Kocbek, M. Gašperlin, Mesoporous silica nanoparticles as delivery carriers: An overview of drug loading techniques, J. Drug Deliv. Sci. Technol. 59 (2020) 101906.
[7] V. Ambrogi, L. Perioli, F. Marmottini, O. Accorsi, C. Pagano, M. Ricci, B. Rossi, Role of mesoporous silicates on carbamazepine dissolution rate enhancement, Micropor. Mesopor. Mater. 113 (2008) 445-452.
[8] G.F. Andrade, D.C.F. Soares, R.K. Almeida, E.M.B. Sousa, Mesoporous silica SBA-16 functionalized with Alkoxysilane groups: preparation, characterization, and release profile study, J. Nanomater. 2012 (2012) 1687-4110.
[9] R. Mellaerts, J.A.G. Jammaer, M. Van Speybroeck, H. Chen, J.V. Humbeeck, P. Augustijns, G. Van den Mooter, J.A. Martens, Physical State of Poorly Water Soluble Therapeutic Molecules Loaded into SBA-15 Ordered Mesoporous Silica Carriers: A Case Study with Itraconazole and Ibuprofen, Langmuir 24 (2008) 8651-8659.
[10] S. Hong, S. Shen, D.C.T. Tan, W.K. Ng, X. Liu, L.S.O. Chia, A.W. Irwan, R. Tan, S.A. Nowak, K. Marsh, R. Gokhale, High drug load, stable, manufacturable and bioavailable fenofibrate formulations in mesoporous silica: a comparison of spray drying versus solvent impregnation methods., Drug. Deliv. 23 (2016) 316-327.
[11] K. Trzeciak, S. Kazmierski, E. Wielgus, M. Potrzebowski, DiSupLo - New extremely easy and efficient method for loading of active pharmaceutical ingredients into the pores of MCM-41 mesoporous silica particles, Micro. Meso. Mater. 308 (2020) 110506-110523.
[12] V. Ambrogi, L. Perioli, C. Pagano, F. Marmottini, M. Moretti, F. Mizzi, C. Rossi, Econazole Nitrate-loaded MCM-41 for an antifungal topical powder formulation, J. Pharm. Sci. 99 (2010) 4738-4745.
[13] E. Skorupska, A. Jeziorna, M. Potrzebowski, Thermal Solvent-free method of loading of pharmaceutical cocrystals into the pores of silica particles: a case of naproxen/picolinamide cocrystal, J. Phys. Chem. C 120 (2016) 13169-13180.
[14] R.J. Ahern, J.P. Hanrahan, J.M. Tobin, K.B. Ryan, A.M. Crean, Comparison of fenofibrate–mesoporous silica drug-loading processes for enhanced drug delivery, Eur. J. Pharm. Sci. 50 (2013) 400-409.
[15] B. Malfait, N. Correia, A. Mussi, L. Paccou, Y. Guinet, A. Hédoux, Solid-state loading of organic molecular materials within mesoporous silica matrix: application to ibuprofen, Micro. Meso. Mater. 277 (2019) 203-207.
[16] B. Malfait, N. Correia, C. Ciotonea, J. Dhainaut, J.-P. Dacquin, S. Royer, N. Tabary, Y. Guinet, A. Hédoux, Manipulating the Physical states of confined ibuprofen in SBA-15 based

drug delivery systems obtained by solid-state loading: impact of the loading degree, J. Chem. Phys. 153 (2020) 154506-13.
[17] B. Malfait, L. Paccou, N. Correia, Y. Guinet, A. Hedoux, Identification of an amorphous-amorphous two-step transformation in indomethacin embedded within mesoporous silicas, Micro. Meso. Mater. 328 (2021) 111502.
[18] Y. Guinet, L. Paccou, F. Danede, A. Hedoux, Confinement of molecular materials using a solid-state loading method: a route for exploring new physicals states and their subsequent transformation highlighted by caffeine confined to SBA-15 pores, RSC Adv. 11(55) (2021) 34564-34571.
[19] F. Balas, M. Manzano, M. Colilla, M. Valler-Regi, L-Trp adsorption into silica mesoporous materials to promote bone formation, Acta Biomater. 4 (2008) 514-522.
[20] M. Colilla, M. Manzano, M. Vallet-Regi, Recent advances in ceramic implants as drug delivery systems for biomedical applications, Int. J. Nanomedicine 3(4) (2008) 403-414.
[21] K.S.W. Sing, D.H. Everett, R.A.W. Haul, L. Moscou, R.A. Pierotti, J. Rouquerol, T. Siemieniewska, Reporting phy-sisorption data for gas solid systems with special reference to the determination of surface area and porosity, Pure Appl. Chem. 57 (1985) 603-619.
[22] X. Huang, N.P. Young, H.E. Townley, Characterization and Comparison of Mesoporous Silica Particles for Optimized Drug Delivery, Nanomater. Nanotechnol. 4 (2014) 1-15.
[23] M. Beinier, G. Rengarajan, S. Pankaj, D. Enke, M. Steinhart, Manipulating the crystalline state of pharmaceuticals by nanoconfinement, Nano Lett. 7(5) (2007) 1381-1385.
[24] F. Babonneau, L. Yeung, N. Steunou, C. Gervais, Solid State NMR characterization of encapsulated molecules in mesoporous silica, J. Sol-Gel Sci. Technol. 31 (2004) 219-223.
[25] L. Pajchel, W. Kolodziejski, Synthesis and characterization of MCM-48/hydroxyapatite composites for drug delivery: Ibuprofen incorporation, location and release studies, Mater. Sci. Eng. C 91 (2018) 734-742.
[26] E. Skorupska, A. Jeziorna, P. Paluch, M. Potrzebowski, Ibuprofen in Mesopores of Mobil Crystalline Material 41 (MCM-41): A Deeper Understanding, Mol. Pharmaceutics 11 (2014) 1512-1519.
[27] K. Trzeciak, S. Kazmierski, K. Druzbicki, M. Potrzebowski, Mapping of Guest Localization in Mesoporous Silica Particles by Solid-State NMR and Ab Initio Modeling: New Insights into Benzoic Acid and p-Fluorobenzoic Acid Embedded in MCM-41 via Ball Milling, J. Phys. Chem. C 125 (2021) 10096-10109.
[28] I.V. Melnyk, G.I. Nazarchuk, M. Václavíková, Y.L. Zub, IR spectroscopy study of SBA-15 silicas functionalized with the ethylthiocarbamidepropyl groups and their interactions with Ag(I) and Hg(II) ions, Appl. Nanosci. 9 (2019) 683-694.
[29] S. Hellstaen, H.Y. Qu, T. Heikkila, J. Kohonen, S.P. Reinikainen, M. Louhi-Kultanen, Raman spectroscopic imaging of indomethacin loaded in porous silica, Cryst. Eng. Comm. 14 (2012) 1582-1587.
[30] A. Hédoux, L. Paccou, Y. Guinet, J.-F. Willart, M. Descamps, Using the low-frequency Raman spectroscopy to analyze the crystallization of amorphous indomethacin, European Journal of Pharmaceutical Sciences 38(2) (2009) 156-164.
[31] A. Hédoux, Recent developments in the Raman and infrared investigations of amorphous pharmaceuticals and protein formulations: a review, Adv. Drug Deliv. Rev. 100 (2016) 133-146.
[32] A. Hédoux, Y. Guinet, P. Derollez, O. Hernandez, R. Lefort, M. Descamps, A contribution to the understanding of the polyamorphism situation in triphenyl phosphite, Phys. Chem. Chem. Phys. 6 (2004) 3192-3199.
[33] J.-F. Willart, M. Descamps, Solid State Amorphization of Pharmaceuticals, Molecular Pharmaceutics 5(6) (2008) 905-920.

[34] F.L. Galeener, P.N. Sen, Theory for the first-order vibrational spectra of disordered solids, Physical Review B 17(4) (1978) 1928-1933.
[35] R. Shuker, R. Gammon, Raman-scattering selection-rule breaking and the density of states in amorphous materials, Physical Review Letters 25(4) (1970) 222-225.
[36] A. Hedoux, P. Derollez, Y. Guinet, A.J. Dianoux, M. Descamps, Low-frequency vibrational excitations in the amorphous and crystalline states of triphenyl phosphite: A neutron and Raman scattering investigation - art. no. 144202, Physical Review B 63(14) (2001) 144202.
[37] A. Frontzek, J. Embs, L. Paccou, Y. Guinet, A. Hédoux, Low-frequency dynamics of BSA complementary studied by Raman and inelastic neutron spectroscopy, J. Phys. Chem. B 121 (2017) 5125-5132.
[38] T. Achibat, A. Boukenter, E. Duval, Correlation effects on Raman scattering from low-energy vibrational modes in glasses. II. Experimental results, Journal of Chemical Physics 99(3) (1993) 2046-51.
[39] E. Duval, A. Boukenter, T. Achibat, Vibrational dynamics and the structure of glasses, Journal of Physics: Condensed Matter 2(51) (1990) 10227-34.
[40] A. Hedoux, Y. Guinet, M. Descamps, Raman signature of polyamorphism in triphenyl phosphite, Physical Review B 58(1) (1998) 31-4.
[41] A. Hédoux, L. Paccou, Y. Guinet, Relationship between b-relaxation and structural stability of lysozyme: microscopic insight on thermostabilization mechanism by trehalose from Raman spectroscopy experiments, J. Chem. Phys. 140 (2014) 225102-7.
[42] C. Görbitz, K. Törnroos, G.M. day, Single-crystal investigation of L-tryptophan with Z'=16, Acta Cryst B 68 (2012) 549-557.